Marine and Petroleum Geology
Volume 121, November 2020, 104615 https://doi.org/10.1016/j.marpetgeo.2020.104615

Stable-isotope and fluid inclusion constraints on the timing of diagenetic events in the dolomitized Dolomia Principale inner platform (Norian, Southern Alps of Italy)

Fabrizio Berra[1], Karem Azmy[2], Giovanna della Porta[1]

[1] Dipartimento di Scienze della Terra "A. Desio", Università degli Studi di Milano, Via Mangiagalli 34, Milano, Italy

[2] Department of Earth Sciences, Memorial University of Newfoundland, St John's, Newfoundland, A1B 3X5, Canada

Keywords: diagenesis, dolomitization, carbonate platform, Triassic, Southern Alps

Abstract

The petrographic, cathodoluminescence (CL), stable isotope, and microthermometry investigation of inner platform facies of the pervasively dolomitized carbonate platform of the Norian (Upper Triassic) Dolomia Principale (Southern Alps, N Italy) identified two major dolomite phases. An early replacement fabric-retentive dolomite (D1 and D2, respectively replacing the sedimentary facies - from fenestral mudstone/wackestone to bioclastic packstone and mudstone and stromatolites- and early marine cements) is followed by a later, vug- and fracture-filling dolomite cement phase (D3, planar-s texture).

The fabric-retentive dolomitized carbonates (< 4 μm−30 μm, D1) and marine fibrous cements (30 μm−250 μm, D2) exhibit dull luminescence under CL whereas the burial dolomite cement (200 μm−500 μm, D3) exhibits zoned luminescence. Microthermometric measurements of the primary two-phase fluid inclusions in D3 yielded a mean homogenization temperature of 112.4 ± 8.2°C. Supposing a surface seawater temperature of at least 20-25°C and a geothermal gradient of about 40°C/km during the Early Jurassic rifting that led to the opening of the Alpine Tethys, such temperature might be reached at reasonable burial depth ranging from 2.0 km to about 2.5 km. According to the subsidence curve this depth, compatible with the temperature recorded by the fluid inclusions, was reached during the Early Jurassic, with D3 cement precipitation causing a significant reduction of the porosity.

The $\delta^{13}C$ values of the investigated dolomites (D1, D2, and D3) show a narrow range of variation (2.0 to 3.1 ‰ VPDB), pointing toward a fluid-buffered system. Differently, the $\delta^{18}O$ values largely varies, ranging from −12.8 to +1.9 ‰ VPDB. In this range, D3 values cluster distinctively between −6.0 to −12.8 ‰ VPDB with respect to D1 and D2, which cluster from about −4 to +1.9 ‰ VPDB. The estimated oxygen isotope composition of the parent fluid of D1 and D2 (~0 to −5 ‰ VSMOW) suggests possible contributions from marine to slightly evaporated seawater, which is consistent with the arid climate and some basin restrictions suggested by earlier studies, whereas that of D3 (+1 to +5 ‰ VSMOW) is consistent with burial fluids.

The followed integrated approach highlights the possibility to better characterize the occurrence of multiple diagenetic events in time and space, as well as their feedback effects on the porosity evolution of dolomitized carbonate reservoirs, framing the diagenetic events at regional scale.

Marine and Petroleum Geology
Volume 121, November 2020, 104615 https://doi.org/10.1016/j.marpetgeo.2020.104615

Introduction

Dolomitized carbonate platforms in the geological record document that efficient post-depositional processes are able to produce large volumes of dolomite (e.g., Zenger et al., 1980; Land, 1985; Machel, 2004). In some cases, dolomitization is fabric destructive, discontinuously spatially distributed and driven by fractures and faults that favored circulation of dolomitizing fluids during burial. Fabric-retentive dolomitization is instead generally limited to specific facies (e.g., peritidal facies) suggesting that environmental conditions during deposition play a role in the efficiency of the dolomitization processes (Land, 1985). In other cases, the entire volume of carbonate platforms is pervasively dolomitized, with possible preservation of the texture of the precursor carbonates (e.g., Frisia and Wenk, 1993). Such pervasive fabric-retentive dolomitization is typically associated with early diagenetic stages of near-surface conditions (e.g., Frisia, 1994) in periods (including the Triassic, e.g., Given and Wilkinson, 1987; Burns et al., 2000) characterized by abundance of dolomite. One of the best case studies of pervasive, fabric-retentive dolomitization of the Phanerozoic is the Norian (Upper Triassic) carbonate succession of Western Tethys. This Norian carbonate succession, cropping out from Sicily to the Apennine, Southern Alps, Northern Calcareous Alps and Transdanubian Range, is known with different names in different regions: Dolomia Principale in the Southern Alps of Italy (Jadoul et al., 1992; Frisia and Wenk, 1993), Maindolomite and Fődolomit in Hungary (Haas and Budai, 1995; Haas et al., 2015), Hauptdolomit in the Northern Calcareous Alps of Austria (since Gümbel, 1857).

The aim of this research is the characterization of the major diagenetic stages recorded by the different types of dolomite phases in a section of the Norian Dolomia Principale of the Southern Alps, in order to provide insights about the diagenetic setting and the timing of the dolomitization events and dolomite cement precipitation. The diagenetic evolution is interpreted considering the present-day knowledge about the dolomitization processes affecting the Dolomia Principale, whose complexity has been the subject of research in the last 50 years, and the basin evolution of the Southern Alps, knowing the burial history of the succession. This study follows a multiproxy approach including petrographic, cathodoluminescence, fluid inclusions, and oxygen and carbon stable isotope analyses. This approach is crucial for a better evaluation of the timing of the diagenetic events and for the understanding of the porosity evolution through time in dolomitized carbonates, from deposition to present-day.

Geological setting

The Norian carbonate succession of Western Tethys represents a thick (up to more than 1500 m in some areas) carbonate platform (Marcoux et al., 1993). The Norian inner platform facies of the Dolomia Principale/Hauptdolomit are bordered landward by coastal deposits documenting arid climate (evaporites and sabkha facies are common in the Norian Gipskeuper in Europe and Grezzoni in the Apennine; e.g.; Ciarapica and Passeri, 1978; Martini et al., 1989; Ziegler, 1990; Shukla et al., 2006) and seaward by calcareous reef facies (Dachstein Limestone and equivalent) passing to open-sea conditions recorded by deep-water nodular limestone (Hallstatt facies; Mandl, 2000). The inner platform belt, representing the major part of this carbonate system is well preserved in different Tethys domains, such as the Apennine, the Alps (Southern Alps; Fig. 1; Austroalpine), Hungary and surrounding areas (Marcoux et al., 1993). In the Southern Alps and part of the Austroalpine Domain, the stratigraphic evolution of the Dolomia Principale records a major extensional stage, documented by the development of fault-controlled basins in the inner platform domain, where massive dolomitic scarp breccia units at the borders of the basins interfingered basinward with

Marine and Petroleum Geology
Volume 121, November 2020, 104615 https://doi.org/10.1016/j.marpetgeo.2020.104615

calciturbidites deposited in anoxic sea-bottoms (Jadoul, 1986; Jadoul et al, 1992; Berra, 1995; Berra and Jadoul, 1999). In the study area, the Lombardy Basin of the Southern Alps, these km-size, fault-controlled, intraplatform troughs have a narrow, dolomitized reef belt dominated by serpulids and microbialites (Berra and Jadoul, 1996). The different biota in reefs facing the intraplatform basins in the Southern Alps with respect to reefs facing the open sea (Dachstein Reef; e.g. Roniewikz et al., 2007) as well as sedimentological evidence suggest restricted conditions in the inner platform domain (i.e.; poor exchange of water with the open sea, high temperature, and evaporation; Berra and Jadoul, 1996; Cirilli et al., 1999). The different chemical and physical characteristics of Norian seawater in the inner platform domain with respect to the Tethys Ocean thus favored the development of distinctive reef frameworks dominated by serpulids and microbialites in the Southern Alps. Furthermore, this environmental setting promoted early diagenetic conditions, favouring the pervasive, fabric-retentive dolomitization of the entire inner platform domain, including the microbialite margin and slope breccias bordering the intraplatform basins (Frisia and Wenk, 1993; Berra and Jadoul, 1996).

The demise of the Dolomia Principale in the Southern Alps is marked by a subaerial exposure at the platform top and the rapid and massive input of clay (close to the Norian-Rhaetian boundary), thickest in the basins (Jadoul et al., 2004; Berra et al., 2010). At the end of the Rhaetian, during which a gradual recovery of carbonate production is observed, the horst and graben paleotopography inherited by the extensional tectonics affecting the Dolomia Principale is smoothed, leading to the development of a new, continuous, carbonate platform system of early Hettangian age (Albenza Formation; Jadoul et al., 2004).

Since late Hettangian, a new extensional event led to the development of a horst-and-graben geometry defining major tectonic domains, consisting of persisting highs and fault-bounded, strongly subsiding, deep-water basins where up to 3 km of cherty limestone (Moltrasio Limestone) were deposited (from West to East, Western Southern Alps high, Lombardy Basin, Trento high, Belluno Basin and Friuli Platform; e.g., Bernoulli, 1964; Bosellini, 1973). In central Lombardy the acme of the extensional tectonics culminated in the Hettangian-Sinemurian, decreasing rapidly close to the Pliensbachian-Toarcian boundary, when a new extensional event affected the western part of the Southern Alps (Bertotti et al., 1993; Berra et al., 2009). The early Jurassic extensional phase evolved into the continental breakup, which led to the opening of the Alpine Tethys (Bertotti et al., 1993). In the Lombardy Basin, the early Jurassic extension was followed by a relative quiescent time interval, with deposition of open sea sediments until the late early Cretaceous, when the first record of siliciclastic input is documented, as well as syn-sedimentary deformation and fold growth (since the latest Albian; Bersezio and Fornaciari, 1994).

Since the late Cretaceous, this succession has been folded and thrust southwards, due to the initial stages of the Alpine orogenic events (Zanchetta et al., 2012).

Methods

Samples from the Dolomia Principale were collected along stratigraphic logs exposed in a well-preserved succession of inner platform facies in the southern part of the Southern Alps (Monte Resegone, Lombardy, Figs. 1-3). Samples are representative of all the sedimentary facies recognized in the inner platform domain. Hand specimens were thin sectioned and stained with a mixture of alizarin red and potassium ferricyanide (Dickson, 1966). Petrographic analyses were carried out on thin sections using a standard polarized light microscope and a cathodoluminoscope. Cathodoluminescence (CL) was performed using a CITL Optical Cathodoluminoscope at the

Marine and Petroleum Geology
Volume 121, November 2020, 104615 https://doi.org/10.1016/j.marpetgeo.2020.104615

University of Milan, Department of Earth Sciences "A. Desio", operated at 14kV accelerating voltage and 0.5 mA gun current intensity.

Double-polished wafers (~80 μm-thick) were prepared for fluid inclusion studies and microthermometric measurements (84 analyses) were performed using a Linkham THMSG600 heating-freezing stage at the Memorial University of Newfoundland. The stage was calibrated using synthetic H_2O and CO_2 fluid inclusion standards and the precision was ±0.2°C at −56.6°C and ±1°C at 300°C. The homogenization temperatures (T_h) were measured in primary two-phase fluid inclusions (Goldstein and Reynolds, 1994) following the procedures outlined in Bodnar (2003). No salinity estimates were possible due to the small size and hazy appearance of the inclusions.

Mirror-image slabs of thin sections were polished, cleaned with de-ionized water and dried at 40°C (e.g., Azomani et al., 2013; Hou et al., 2015). Representative samples from different dolomite generations were microdrilled from the slabs under a binocular microscope with a low-speed microdrill.

Stable isotope (oxygen and carbon) analyses of 44 carbonate powder samples were performed using an automated carbonate preparation device (GasBench II) connected to a Delta V Advantage (Thermo Fisher Scientific Inc.) isotopic ratio mass spectrometer at the Department of Earth Sciences "A. Desio", University of Milan. Carbonate powders (about 200 m μg each) were reacted with > 99 % orthophosphoric acid at 70°C. The carbon and oxygen isotope compositions are expressed in the conventional delta notation calibrated to the Vienna Pee-Dee Belemnite (V-PDB) scale by the international standards IAEA 603 and NBS-18. Analytical reproducibility for these analyses was better than ± 0.1‰ for both $\delta^{18}O$ and $\delta^{13}C$ values.

Results

Facies analyses, and petrographic-diagenetic characterization

The inner platform facies of the Dolomia Principale (Fig. 2) are characterized by a bedded carbonate succession commonly organized in shallowing-upward cycles, capped by stromatolitic beds (Fig. 3). They are entirely dolomitized. The investigated facies at the Monte Resegone consist of a succession of dolomitized subtidal mudstone/wackestone at the base of the cycle, overlain by intra-bioclastic wackestone/packstone and, eventually, by a few centimeters thick (2 to 40 cm on average) intertidal fenestral laminated microbial boundstone (stromatolite). Shallowing-upward cycles are about 2 to 10 m-thick. Subtidal intervals are frequently rich in skeletal components, including bivalves (also large megalodontids), gastropods, foraminifera, and dasyclad algae (Fig. 3).

Petrographic analysis documents extensive dolomitization (Fig. 4) affecting all the samples independently from their facies type, from subtidal mudstone, wackestone and bioclastic/intraclastic packstone to intertidal fenestral laminated microbial boundstone (Fig. 4 a). The dolomitization is fabric-retentive: it preserves also subtle fabric details (Fig. 4e); less commonly, subtidal mudstone is strongly recrystallized, with the growth of dolomite crystals (50 — 500 μm crystal sizes) with a cloudy core and transparent rims (Fig. 4f).

Dolomite 1 (D1) is fabric-retentive (Fig. 5) and the most abundant (ca. ≥ 80 % by volume). It replaces entirely, preserving the original texture, the precursor mudstone, wackestone, packstone and fenestral microbial boundstone (Fig. 5) and is crosscut by microstylolites and fractures. It is dolomicrite to dolomicrosparite (<4 — 30 μm) and is dull to non-luminescent (Fig. 5).

Dolomite 2 (D2) is the least abundant phase: qualitatively evaluated in less than ca. 5 % per area in thin section on average, it is only locally higher, when depositional intraparticle and interparticle porosity is abundant (Fig. 4a–d). D2 consists of cloudy, inclusion-rich, fabric-retentive

Marine and Petroleum Geology
Volume 121, November 2020, 104615 https://doi.org/10.1016/j.marpetgeo.2020.104615

dolomitized crystals (Fig. 4d) that replaced marine precursor fibrous calcite/aragonite cements. These dolomitized cements, filling the primary inter- and intraparticle and fenestral porosity grew on a substrate such as lining the fenestrae in stromatolites, have a crystal length up to 0.25 mm and appear dull to non-luminescent (Fig. 5).

Dolomite 3 (D3) postdates D2 and consists of planar-s (subhedral) pore- and fracture-filling dolomite cement (up to ca. ~ 10 % volume; Fig. 5) with coarser crystals than D1 and D2 (up to more than 0.5 mm in size) that appear relatively transparent under plane polarized light. Under CL, D3 results zoned, bright luminescent, at the contact with D2, gradually and seamless changing into dull luminescence towards the center of the pore (i.e., during the crystal growth; Fig. 5). The bright luminescent part of the D3 cement has the same response to CL of the dolomite cement filling fractures.

The intertidal (e.g., fenestral laminated microbial boundstone) and subtidal bioclastic facies commonly contain primary intraparticle and interparticle, fenestral and growth framework pores partially or entirely occluded by different generations of dolomitic cements (D2 and D3; Fig. 4a, c, d). Both D2 and D3 occur within intraparticle pores (mostly fossils, bivalves and dasyclad algae) and intraparticle porosity (such as in the fenestral/shrinkage pores). D3 also occur in fractures (secondary porosity). Depositional porosity is up to about 20% in stromatolitic boundstone (where it occurs as interlaminae and fenestral millimeter-size pores), but it can be observed in almost all the grainy facies. The depositional pores are invariably rimmed by the cloudy, inclusion-rich, fibrous non luminescent dolomitized crystals (D2). D2 occurs as continuous rims from 0.2 to 0.4 mm thick on average, thus part of the depositional porosity is preserved in millimeter-size pores. Later, planar-s dolomite cement (D3) precipitate in the remaining porosity, filling it completely or, less frequently, partially. When cements D3 do not completely fill the pores, a residual porosity (volumetrically reduced, not more than 1% when present) can be observed. Only rarely, younger, post-D3 cements can be found.

Carbon and oxygen stable isotopes

The results of the measured C and O isotopes of the investigated dolomites are listed in Table 1 and their statistics are summarized in Table 2. The $\delta^{13}C$ values of the investigated dolomite phases (D1 to D3) vary slightly between 2.0 ‰ and 3.1‰ being fairly uniform for all the dolomite phases, whereas $\delta^{18}O$ values vary significantly from −12.8 to +1.9 ‰ (Fig. 6). The oxygen stable isotope compositions of D1 and D2 largely overlap (−1.3 to −0.1 ‰), whereas that of D3 is distinctively ^{18}O depleted (average around -9.3 ‰; Fig. 6; Table 1).

Fluid inclusions

Primary two-phase aqueous fluid inclusions were examined in the dolomite phase D3 (Table 3). No measurable inclusions were available in D1 (dolomitized facies) or D2 (fibrous cement crystals). Primary two-phase (liquid + vapor) inclusions, mainly in clusters and showing no stretching, were selected for measurements. The measured inclusions, generally ≤ 10 µm, had consistent liquid:vapor ratios (~0.95) and their homogenization temperatures (T_h, the minimum estimate of entrapment temperature-temperature at which the vapor bubble disappears) are listed in Table 3 and presented in Figure 7. The mean T_h value (Table 3) of D3 is 112 ± 8°C (n = 84).

Marine and Petroleum Geology
Volume 121, November 2020, 104615 https://doi.org/10.1016/j.marpetgeo.2020.104615

Interpretation and discussion

Dolomitization and dolomite cement precipitation

Petrographic and CL observations of the Dolomia Principale dolomites suggest that dolomitization started at early stages of diagenesis as a pervasive event, affecting skeletal components, sediments (D1) and early marine cements (D2). Dolomitization was followed by a later phase of precipitation of dolomite cement (D3) partly to totally filling the depositional porosity and fractures, suggesting that the fluid precipitating D3 moved along this network, postdating the D2 dolomitization of the early marine cements. No evidence of meteoric dissolution has been observed, thus excluding a significant meteoric alteration before dolomitization. The fabric-retentive dolomicrite (D1), dull in CL (Fig. 4, 5) supports an early stage of pervasive dolomitization of marine facies at near-surface conditions. The preservation of the fibrous texture of precursor marine cement of the non-luminescent D2 (Fig. 4, 5) is also consistent with pervasive early dolomitization processes that affected both the sediments and fibrous cements during the same dolomitization event. This early dolomitization scenario in the Dolomia Principale has been suggested by previous diagenetic studies (e.g.; Frisia and Wenk, 1993; Frisia, 1994; Meister et al., 2015) that ascribe dolomitization to different processes (i.e.; reflux, hypersaline sabkha-like conditions, microbial dolomite model) along with possible existence of limited/local primary dolomites (restricted locations) by direct precipitation from seawater (Meister and Frisia, 2019).

The early origin of dolomitization D1 and D2 is constrained also by sedimentological evidence, related to the geodynamic scenario existing at the time of deposition of the Dolomia Principale in the Southern Alps and Hauptdolomit in the Austroalpine. Several studies (Frisia and Wenk, 1993; Frisia, 1994; Iannace and Frisia, 1994; Cirilli et al., 1999; Meister et al., 2013; Meister and Frisia, 2019) suggest that paleogeography and climate played a major role in promoting the pervasive dolomitization, which started shortly after deposition, of the carbonate deposits of the Western Tethys.

Important constraints on the timing of the dolomitization can be obtained from the fact that, due to an early Jurassic extensional tectonic, the Dolomia Principale and Hauptdolomit were exposed on fault-controlled escarpments, triggering breccia deposits in the Lower Jurassic succession. The clasts from the Dolomia Principale and Hauptdolomit embedded in Lower Jurassic basinal cherty limestone are dominantly dolomites, which suggests that a fabric-retentive dolomitization event of the entire Norian platform occurred before the Early Jurassic, both in the Southern Alps and in the Central Austroalpine (respectively, Wiedenmayer, 1963; Eberli, 1992). Furthermore, the carbonates, alternating with claystone, overlying the Dolomia Principale are mainly calcareous: the upper boundary of the Dolomia Principale is sharp, locally unconformable and marked by subaerial exposure (Berra et al., 2010; Berra, 2012). Where the carbonates above the Dolomia Principale are dolomitized, this dolomitization is local and typically destructive, thus different from the pervasive, fabric-retentive dolomitization that characterizes the Norian Dolomia Principale carbonate platform. The different dolomitization processes in the Norian vs. Rhaetian successions (Iannace and Frisia, 1994) suggest that the early diagenetic fabric-retentive dolomitization of the inner platform facies of the extensive Norian carbonate platform (Dolomia Principale, Hauptdolomit and Maindolomite) started shortly after sediment deposition in near-surface settings, and that this process was no more active during the Rhaetian (Iannace and Frisia, 1994).

The efficient Norian fabric-retentive early dolomitization suggests a control by a combination of climatic and paleogeographic conditions (Cirilli et al., 1999). During the Norian arid climate conditions existed in the Western Tethys (Sellwood and Valdes, 2006) where reef and backreef facies (Dachstein Limestone, facing the Tethyan Ocean to the east) and basinal facies (Hallstatt

Marine and Petroleum Geology
Volume 121, November 2020, 104615 https://doi.org/10.1016/j.marpetgeo.2020.104615

Limestone) are calcareous, whereas the inner platform facies (Dolomia Principale-Hauptdolomit) are dolomitized, documenting different, environmentally-controlled early diagenetic conditions. The fact that in the Norian fault-controlled intraplatform troughs of the Lombardy Basin (Jadoul, 1986; Jadoul et al., 1992) and Austroalpine (Berra, 1995) the distal, deep-water basinal resedimented facies are not dolomitized indicates that dolomitization was facies-related, affecting shallow-water succession but exempting deep-water, low-porosity, basinal limestones (e.g., Jadoul et al., 1986; 1992).

The development in the inner platform domain of fault-controlled intraplatform troughs bordered by serpulid and microbialite reefs reflects stressed environmental conditions (Berra and Jadoul, 1996; Cirilli et al., 1999), differently from the oceanward margin of the Norian Platform (Dachstein Reef), where the reef-building biota were dominated by corals and sponges (e.g.; Flügel, 1981). The association of arid climate and a wide inner platform poorly connected with the open sea likely developed anomalous salinity and warm seawater causing stressed environmental conditions that prevented the development of Dachstein-type Norian reef associations, substituted in the Lombardy Basin of the Southern Alps by serpulids and microbialites (Cirilli et al., 1999). Physical and chemical seawater conditions and dry climate likely promoted the replacive dolomitization, in a single event, of the sediments and early marine cements, likely aragonite or high-Mg calcite (Meister et al., 2015).

The coarse crystals of the D3 late pore- and fracture-filling zoned CL cement (Fig. 5) suggest precipitation of dolomite under higher temperature, relative to those of the earlier D1 and D2, in burial settings, but not high enough to promote the precipitation of saddle dolomite. Saddle dolomite is supposed to form at a temperature not less than 90°C up to more than 160°C in highly saline fluids (Spötl and Pitman, 1998). Therefore, the absence of saddle dolomite in D3, which precipitated at the estimated temperature of 100-120°C (the cooler part of the temperature window for the precipitation of saddle dolomite) may suggest that the burial brines precipitating D3 dolomite cement were saline.

The CL zoning of D3 crystals reflects the variations in the manganese (Mn^{+2}, activator of bright luminescence) and iron (Fe^{+2}, a quencher causing dull luminescence in carbonates; Machel and Burton, 1991) molar ratio in the D3 parent diagenetic fluid during D3 cement precipitation. The formation of D3 cement is consistent with the T_h values (112 ± 8°C; Table 3; Fig. 7) of the primary two-phase fluid inclusions entrapped by the cement. Due to the scarcity and small size of post-D3 dolomite types, no specific investigations have been performed.

Insights from carbon and oxygen stable isotopes

The $\delta^{13}C$ values of the investigated dolomites (Fig. 6) overlap and vary only slightly, thus suggesting that the C-isotope composition of the parent dolomitizing fluid(s) was buffered by that of the precursor marine carbonates and there was no influence of organic matter. $\delta^{13}C$ values fit with the proposed carbon isotope values proposed for Norian marine carbonates (Veizer et al., 1999; Korte et al., 2005). Unlike D3, the C- and O-isotope compositions of D1 and D2 overlap considerably and mostly fall within the documented range of the best-preserved Triassic marine limestone (Veizer et al., 1999; Korte et al., 2005). This supports that the platform interior facies (D1) and fibrous marine cements (D2) were dolomitized at near-surface conditions, which is consistent with the conclusions from their petrographic features. Frisia (1994) suggested that the dolomitizing fluids were provided by the cyclic subaerial exposure of the Dolomia Principale, allowing saline fluid circulation through the sediments.

Marine and Petroleum Geology
Volume 121, November 2020, 104615 https://doi.org/10.1016/j.marpetgeo.2020.104615

Early dolomitization may occur by dolomitizing fluids formed from a mixture of meteoric and seawater, which is associated with significant changes in the $\delta^{18}O$ values of the produced dolomites compared to those of the precursor (e.g, Azomani et al., 2013; Olanipekun et al., 2014; Hou et al., 2015). On the contrary, the similar O-isotope compositions of D1 and D2 with those of the best-preserved Triassic marine carbonates (Fig. 6) suggest that the dolomitizing fluid(s) had significant contributions from the Triassic marine water from which the carbonate facies (replaced by D1) and the fibrous cement (replaced by D2) precipitated.

Unlike the $\delta^{13}C$, the $\delta^{18}O$ values of D3 are low (−9.3 ± 0.2 ‰ VPDB; Table 2) and plot separately in a cluster distinctive from those of D1 and D2 (Fig. 6). This supports that D3 precipitated at higher temperature in deeper burial settings, which is consistent with the T_h values of D3 (112 ± 8°C; Table 3).

The oxygen isotopic composition of dolomites is influenced by that of the dolomitizing fluid, because dolomitization requires large supply of Mg-rich fluids, and by the temperature of dolomitization (Land, 1983; 1992). The $\delta^{18}O$ value of the parent dolomitizing fluid can be calculated by using the T_h values of primary two-phase fluid inclusions entrapped into the dolomite crystals (Goldstein and Reynolds, 1994).

The fabric retention and preservation of the micritic grain size (D1) and fibrous crystals (D2) are also consistent with early dolomitization of near-surface conditions (T = 25–30°C). Thus, the oxygen isotope composition of D1 and D2 (+1.7 to −3.9 VPDB ‰, Table 2) suggests a parent dolomitizing fluid with $\delta^{18}O_{D1\text{-}D2\ fluid}$ values between 0 to -5 VSMOW ‰ (Fig. 8). Both sedimentological evidence (e.g.; Jadoul et al., 1992; Berra and Jadoul, 1996) and paleogeographic constraints (Marcoux et al., 1993) indicate that investigated dolomitized inner platform facies were deposited in tropical conditions with arid climate. The estimated $\delta^{18}O_{SW}$ value of tropical Triassic seawater is between −1 and −4 ‰ VSMOW (Friedman and O'Neil, 1977; Veizer et al., 1999; Korte et al., 2005). Thus, the lower end-member values of the $\delta^{18}O_{D1\text{-}D2\ fluid}$ range (Fig. 8) falls within the range of the $\delta^{18}O_{SW}$ but the high end-member values are slightly more enriched and barely exceeds the $\delta^{18}O_{SW}$ range by ~ 1 ‰ (Fig. 8), which may suggest contributions from evaporated marine water (cf. Frisia, 1994). This is further consistent with the suggested scenario of arid climate and basin restrictions reconstructed from the sedimentological evidence: the Norian carbonate platform of the Dolomia Principale was bordered by sabkha evaporitic facies (Norian Burano Anhydrite in Central Italy; Martini et al., 1989) and by coastal and continental fluvial to playa environments (Norian Keuper, Germany) in semi-arid to arid climate (Shukla et al., 2006).

The high T_h values of D3 (Table 3) indicate a parent fluid precipitating the dolomite in pores and fractures more enriched in ^{18}O, with $\delta^{18}O$ values between +1 and +5 ‰ VSMOW (Fig. 8), which are expected for fluids of deep burial settings (e.g., Azmy et al., 2001; Azomani et al., 2013, Hou et al., 2015). The O isotope composition of the parent fluid of the D3 cement is different from its counterparts of the early replacive D1 and D2, suggesting that it was a fluid present in the basin during burial, likely moving through fractures and the fault system developed by rifting during the Early Jurassic (cf. Bertotti et al., 1993).

Timing of diagenetic events: constraints form D3 dolomite

The data about the temperature of D3 dolomite and the knowledge of the regional burial evolution of the studied succession (Fig. 9) may provide constraints about the timing of D3 dolomite cement precipitation.

An estimate for the depth of precipitation of D3 can be suggested if heat flow and thermal conductivity values could be established and a reliable geothermal gradient could be defined. The

Marine and Petroleum Geology
Volume 121, November 2020, 104615 https://doi.org/10.1016/j.marpetgeo.2020.104615

heath flow (Q) in the Southern Alps is considered to have increased from values around 60 mW/m^2 during the Norian to > 100 mW/m^2 in the Early Jurassic (Ceriani et al., 2006), when a rifting stage affected the domain (Bertotti et al., 1993), increasing the heath flow and, thus, the geothermal gradient. Based on the lithology of the succession (mainly dolomite, limestone and shale), the estimated maximum thermal conductivity (c) is expected to be ~ 2.5 W/mK at 300°K (Robertson, 1988,) but it decreases with increasing temperature (Vasseur et al., 1995). Assuming that the bedded basinal cherty lime mudstone (Moltrasio Limestone) that fills the Jurassic rifting basins has high porosity (with low permeability), a realistic average geothermal gradient (dT/dZ=Q/c; Bjorlykke, 2015) ranging from ~ 25°C/km (at a heat flow ~ 60 mW/m^2 before rifting) to 40°C/km during the Early Jurassic rifting (at a heath flow of ~ 100 mW/m^2) can be suggested. Therefore, the T_h values of D3 (97−130°C; 112.4 ± 8.2°C) may suggest dolomite precipitation at depths of 2.5 to 3 km during the Early Jurassic, considering surface temperatures of a few degrees. During the initial stages of burial, a surface temperature of at least 20 to 25°C can be suggested, compatible with the shallow tropical settings existing in the Southern Alps of Italy until the early Hettangian: this scenario suggests that D3 dolomite precipitation likely occurred at shallower depth, likely between 2.0 to 2.5 km. It is assumed that rock and fluid had the same temperature because the absence of typical crystal fabric (e.g.; zebra and saddle dolomite) and fault-controlled distribution of dolomitized volumes within limestone successions (cf., Davies and Smith, 2006 and references therein) exclude a hydrothermal origin for D3.

Extensional tectonics generally produces predominantly vertical fracture networks, which may serve as conduits for pore water (Bjørlykke, 2015). The D3 dolomite precipitated from fluids moving along fractures in an already dolomitized succession, filling the primary porosity preserved after the precipitation of the early marine dolomitized (D2) cements and the extensional fractures. With these assumptions and based on the subsidence curves for the Southern Alps (Berra and Carminati, 2010), a depth of about 2.0 to 2.5 km (required to obtain a temperature of about 110°C) was reached during the early Jurassic (Fig. 9). Accepting this interpretation, the fractures that drove the fluid migration responsible for the precipitation of D3 were likely related to extension during the Jurassic rifting stage recorded in the Southern Alps, which is consistent with the measured T_h values and a geothermal gradient of about 40°C/km.

Conclusions

Petrographic examinations of the Norian Dolomia Principale in the Southern Alps of Italy indicate extensive dolomitization and reveal two main dolomite phases (D1-D2 and D3): early facies replacive fabric-retentive dolomicrite and dolomicrosparite (D1) and dolomitized fibrous cements of precursor marine origin (D2) and a late planar-s vug- and fracture-filling dolomite cement (D3).

Petrographic features of D1 and D2 suggest an early dolomitization event at near-surface conditions (nearly 25 – 30°C as expected for tropical latitudes) by dolomitizing fluids that were a mixture of marine and evaporated seawater, according to the measured $\delta^{18}O$ values and compatible with the paleogeographic scenario. The petrographic, CL and stable oxygen isotope features of D3 reflect precipitation at later stages of diagenesis during burial, which are consistent with the high T_h values (112.4 ± 8.2°C) estimated through aqueous fluid inclusions and the calculated estimates of its parent fluid oxygen isotope composition (+1 to +5‰ VSMOW).

The T_h values of D3 suggest precipitation at a depth of 2 km to around 2.5 km using an estimated geothermal gradient of about 40°C/km, expected during the Early Jurassic rifting.

Marine and Petroleum Geology
Volume 121, November 2020, 104615 https://doi.org/10.1016/j.marpetgeo.2020.104615

These results thus constrain the D1-D2 dolomitization stage before the Early Jurassic (near surface dolomitization), confirming the early origin of the fabric-retentive dolomitization (Frisia and Wenk, 1993; Frisia, 1994; Iannace and Frisia, 1994) and document that the D3 planar-s dolomite cements precipitated from fluids moving along fractures generated during the Early Jurassic rifting stage. The results here reported indicate that most of the porosity of the Dolomia Principale was occluded in the early Jurassic, with fluids moving along fractures likely related to the extensional tectonics. After this early Jurassic event, only a reduced residual porosity persisted.

Acknowledgements

The Authors would like to thank Daniele De Vita for the support during field work and laboratory analyses during his MSc thesis. We would like to thank Curzio Malinverno for thin section preparation and Elena Ferrari for stable isotope analyses (University of Milan). The authors would like to thank two anonymous reviewers for their useful comments and the Editor for his support.

References

Azmy, K., Veizer, J., Misi, A., de Oliveira, T.F., Sanches, A.L., Dardenne, M.A., 2001. Dolomitization and isotope stratigraphy of the Vazante Formation, Sao Francisco Basin, Brazil. Precambrian Res. 112 (3), 303-329.

Azomani, E., Azmy, K., Blamey, N., Brand, U., Al-Aasm, I., 2013. Origin of Lower Ordovician dolomites in eastern Laurentia: Controls on porosity and implications from geochemistry. Marine and Petroleum Geology 40, 99-114.

Bernoulli, D. 1964. Zur Geologie des Monte Generoso (Lombardische Alpen), Beitr. Geol. Karte Schweiz., 118, pp. 135.

Berra, F., 1995. Stratigraphic evolution of a Norian intraplatform basin recorded in the Quattervals Nappe (Austroalpine, Northern Italy) and paleogeographic implications, Eclogae Geol. Helv. 88, 501–528.

Berra, F., 2012. Sea-level fall, carbonate production, rainy days: how do they relate? Insight from Triassic carbonate platforms (Western Tethys, Southern Alps, Italy). Geology 40, 271-274.

Berra, F., Carminati, E., 2010. Subsidence history from a backstripping analysis of the Permo-Mesozoic succession of the Central Southern Alps (Northern Italy). Basin Research 22, 952-975.

Berra, F., Jadoul, F., 1996. Norian serpulid and microbial bioconstructions: Implication for the platform evolution in the Lombardy Basin (Southern Alps, Italy). Facies 35, 143-162.

Berra, F., Jadoul, F., 1999. Stratigraphy, paleogeography and tectonic setting of the Norian succession of the Ortles Nappe (Central Austroalpine, Lombardy, Northern Italy). Mem. Sci. Geol. Padova 51, 78-89.

Berra, F., Galli, M. T., Reghellin, F., Torricelli, S., Fantoni, R. 2009. Stratigraphic evolution of the Triassic–Jurassic succession in the Western Southern Alps (Italy): the record of the two-stage rifting on the distal passive margin of Adria. Basin Research. 21, 335-353.

Berra, F., Jadoul, F., Anelli, A., 2010. Environmental control on the end of the Dolomia Principale/Hauptdolomit depositional system in the central Alps: coupling sea-level and climate changes. Palaeogeography, Palaeoclimatology, Palaeoecology 290, 138-150.

Bersezio, R., Fornaciari, M., 1994. Syntectonic Upper Cretaceous deep-water sequences of the Lombardy Basin (Southern Alps, Northern Italy). Eclogae Geol. Helv., 87, 833–862

Marine and Petroleum Geology
Volume 121, November 2020, 104615 https://doi.org/10.1016/j.marpetgeo.2020.104615

Bertotti, G., Picotti, V., Bernoulli, D., Castellarin, A., 1993. From rifting to drifting: tectonic evolution of the South-Alpine upper crust from the Triassic to the Early Cretaceous. Sedimentary Geology 86, 53-76.

Bjorlykke, K., 2015. Petroleum geoscience: From sedimentary environments to rock physics. Springer Science Business Media, 508 pp.

Bodnar, R.J., 2003. Interpretation of data from aqueous-electrolyte fluid inclusions. In: Samson, I., Anderson, A., Marshal, D. (Eds.), Fluid Inclusions: Analyses and Interpretation. Short Course Series, vol. 32. Mineralogical Association of Canada, pp. 81-100.

Bosellini, A., 1973. Modello geodinamico e paleotettonico delle Alpi Meridionali durante il Giurassico-Cretacico. Sue possibili applicazioni agli Appennini. In: Accordi, B. (Ed), Moderne vedute sulla Geologia Dell'Appennino. Quaderni dell'Accademia Nazionale dei Lincei, 183, 163-205.

Burns, S. J., Mckenzie, J. A., Vasconcelos, C., 2000. Dolomite formation and biogeochemical cycles in the Phanerozoic. Sedimentology 47, 49-61.

Ceriani, A., Di Giulio, A., Fantoni, R., Scotti, P., 2006. Cooling in rifting sequences during increasing burial depth due to heat flow decrease. Terra Nova 18, 365-371.

Ciarapica, G., Passeri, L., 1978. I Grezzoni del nucleo apuano; nascita, sviluppo e morte di una piattaforma carbonatica iperalina. Bollettino della Societa Geologica Italiana 97, 527-564.

Cirilli, S., Iannace, A., Jadoul, F., Zamparelli, V., 1999. Microbial-serpulid build-ups in the Norian-Rhaetian of the western Mediterranean area: ecological response of shelf margin communities to stressed environments. Terra Nova 11, 195-202.

Davies, G. R., Smith Jr, L. B., 2006. Structurally controlled hydrothermal dolomite reservoir facies: An overview. AAPG bulletin, 90(11), 1641-1690.

Dickson, J.A.D., 1966. Carbonate identification and genesis as revealed by staining. Journal of Sedimentary Research 36, 491-505.

Eberli, G. P., 1988. The evolution of the southern continental margin of the Jurassic Tethys Ocen as recorded in the Allgäu Formation of the Austroalpine Nappes of Graubünden (Switzerland). Eclogae Geologicae Helvetiae 81, 175-214.

Flügel, E., 1981. Paleoecology and facies of Upper Triassic reefs in the Northern Calcareous Alps, in: Toomey, D. F. (Ed.), European Fossil Reef Models (), SEPM Spec. Publ. 30, 291– 359.

Friedman, I., O'Neil, J.R. 1977. Data of geochemistry: compilation of stable isotope fractionation factors of geochemical interest. Vol. 440. US Government Printing Office.

Frisia, S., 1994. Mechanisms of complete dolomitization in a carbonate shelf: comparison between the Norian Dolomia Principale (Italy) and the Holocene of Abu Dhabi Sabkha, in: Purser, B. , Tucker, M. and Zenger, D. (Eds): A Volume in Honour of Dolomieu (Eds), IAS Spec. Publ., 21, 55–74.

Frisia, S., Wenk, H.-R., 1993. TEM and AEM study of pervasive, multi-step dolomitization of the upper Triassic Dolomia Principale (Northern Italy). J. Sed. Petrol. 63, 1049–1058.

Given, R. K., Wilkinson, B. H., 1987. Dolomite abundance and stratigraphic age; constraints on rates and mechanisms of Phanerozoic dolostone formation. Journal of Sedimentary Research 57, 1068-1078.

Goldstein, R.H., Reynolds, T.J., 1994. Systematics of fluid inclusions in diagenetic minerals. Short course 31, SEPM (Society for Sedimentary Geology). 199 pp.

Gümbel, C.W., 1857. Untersuchungen in den bayerischen Alpen zwischen Isar und Salzach. Jahrb. K.K Geol. Reich. 7, 146–151.

Marine and Petroleum Geology
Volume 121, November 2020, 104615 https://doi.org/10.1016/j.marpetgeo.2020.104615

Haas, J., Budai, T., 1995. Upper Permian-Triassic facies zones in the Transdanubian Range. Rivista Italiana di Paleontologia e Stratigrafia. 101, 249-266.

Haas, J., Lukoczki, G., Budai, T., Demény, A., 2015. Genesis of upper Triassic peritidal dolomites in the Transdanubian Range, Hungary. Facies. 61, 8.

Hou, Y., Azmy, K., Berra, F., Jadoul, F., Blamey, N.J.F., Gleeson, S.A., Brand, U. 2015. Origin of the Esino and Breno dolomites in the Western Southern Alps (Italy): Implications for a volcanic influence. Marine and Petroleum Geology. 69, 38-52.

Iannace, A., Frisia, S., 1994. Changing dolomitization styles from Norian to Rhaetian in the southern Tethys realm. In Dolomites: A Volume in Honour of Dolomieu (Vol. 21, pp. 75-89). IAS Spec. Publ.

ISPRA, 2012. Foglio 076 Lecco. Carta Geologica d'Italia alla scala 1: 50.000, con Note Illustrative (A. Bini, M. Gaetani, L. Zuccoli, A. Piccin, S. Rossi, R. Rossi, M. Cetti, O. Sules, A. Montanari, L. Quaglia, F. Berra, M. Guglielmin, D. Mazzoccola, E. Sciesa, D. Sciunnach, G.B. Siletto, S. Rossi).

Jadoul, F., 1986. Stratigrafia e paleogeografia del Norico nelle Prealpi Bergamasche occidentali. Rivista Italiana di Paleontologia e Stratigrafia. 91, 479–512.

Jadoul, F., Berra, E, Frisia, S., 1992. Stratigraphic and paleogeographic evolution of a carbonate platform in an extensional tectonic regime: the example of the Dolomia Principale in Lombardy (Italy): Rivista Italiana di Paleontologia e Stratigrafia. 98, 29-44.

Jadoul, F., Galli, M. T., Berra, F., Cirilli, S., Ronchi, P., Paganoni, A., 2004. The Late Triassic-Early Jurassic of the Lombardy Basin: stratigraphy, palaeogeography and palaeontology. Field guide book excursion P86. In International Geological Congress.

Korte, C., Kozur, H.W. Veizer, J., 2005. $\delta^{13}C$ and $\delta^{18}O$ values of Triassic brachiopods and carbonate rocks as proxies for coeval seawater and paleotemperature, Paleogeogr. Paleoclim. Paleoecol. 226, 287-306.

Land, L.S., 1983. The application of stable isotopes to studies of the origin of dolomite and to problems of diagenesis of clastic sediments, in: Arthur, M.A., Anderson, T.F., Kaplan, I.R., Veizer J., Land, L.S. (Eds.), Stable isotopes in sedimentary geology. SEPM Short Course Notes 10, p. 4-1– 4-22.

Land, L. S., 1985. The origin of massive dolomite. Journal of Geological Education, 33, 112-125.

Land, L.S. 1992. The dolomite problem: stable and radiogenic isotope clues, in: Clauer, N., Chaudhuri, S. (Eds.), Isotopic Signature of Sedimentary Records. Lecture Notes in Earth Science. 43, 49-68.

Machel, H.G., 2004. Concepts and models of dolomitization: a critical reappraisal, in: Braithwaite, C.J.R., Rizzi, G., Darke, G. (Eds.), The Geometry and Petrogenesis of Dolomite Hydrocarbon Reservoirs. Geological Society London Special Publications. 235, 7-63

Machel, H. G., Burton, E. A. (1991). Causes and spatial distribution of anomalous magnetization in hydrocarbon seepage environments. Am. Assoc. Petrol. Geol. Bull. 75, 1864-1876.

Mandl, G. W., 2000. The Alpine sector of the Tethyan shelf–Examples of Triassic to Jurassic sedimentation and deformation from the Northern Calcareous Alps. Mitteilungen der Österreichischen Geologischen Gesellschaft. 92, 61-77.

Marcoux, J., Baud, A., Ricou, L.E., Gaetani, M., Krystyn, L., Bellion, Y., Guiraud, R., Besse, J., Gallet, Y., Jaillard, E., Moreau, C., Theveniaut, H., 1993. Late Norian (215 to 212 Ma), in: Dercourt, J., Ricou, L.E., Vrielynck, B. (Eds.), Atlas of Tethys palaeoenvironmental maps. Gauthier-Villars. 35–53.

Martini, R., Gandin, A., Zaninetti, L., 1989. Sedimentology, stratigraphy and micropaleontology of the Triassic evaporitic sequence in the subsurface of Boccheggiano and in some outcrops of southern Tuscany (Italy). Rivista italiana di Paleontologia e Stratigrafia. 95, 3-28.

Marine and Petroleum Geology
Volume 121, November 2020, 104615 https://doi.org/10.1016/j.marpetgeo.2020.104615

Meister, P., Frisia, S. 2019. Dolomite formation by nanocrystal aggregation in the Dolomia Principale of the Brenta Dolomites (Northern Italy). Rivista Italiana di Paleontologia e Stratigrafia (Research In Paleontology and Stratigraphy). 125, 183-196.

Olanipekun, B.J., Azmy, K., Brand, U., 2014. Dolomites of the Boat Harbour Formation in the Northern Peninsula, western Newfoundland, Canada: Implications for dolomitization history and porosity control. AAPG Bull. 98, 765-791.

Price, G. D., Twitchett, R. J., Wheeley, J. R., Buono, G., 2013. Isotopic evidence for long term warmth in the Mesozoic. Scientific reports. 3, 1438.

Robertson, E.C., 1988. Thermal properties of rocks. United States Department of the Interior Geological Survey. Open-File Report. 88-441.

Roniewicz, E., Mandl, G. W., Ebli, O., Lobitzer, H., 2007. Early Norian scleractinian corals and microfacies data of the Dachstein Limestone of Feisterscharte, southern Dachstein Plateau (northern Calcareous Alps, Austria). Jahrbuch der Geologischen Bundesanstalt 147, 577-594.

Sellwood, B. W., Valdes, P. J., 2006. Mesozoic climates: General circulation models and the rock record. Sedimentary geology. 190, 269-287.

Shukla, U.K., Bachmann, G.H., Beutler, G., Barnasch, J., Franz, M., 2006. Extremely distal fluvial sandstone within the playa system of Arnstadt Formation (Norian, Late Triassic), Central Germany. Facies. 52, 541–554.

Spötl, C., Pitman, J.K. ,1998. Saddle (baroque) dolomite in carbonates and sandstones: a reappraisal of a burial-diagenetic concept. Spec Publ Int. 26, 437-460.

Vasseur, G., Brigaud, F., Demongodin, L., 1995. Thermal conductivity estimation in sedimentary basins. Tectonophysics. 244, 167-174.

Veizer, J., Ala, D., Azmy, K., Bruckschen, P., Bruhn, F., Buhl, D., Carden, G., Diener, A., Ebneth, S., Goddris, Y., Jasper, T., Korte, C., Pawellek, F., Podlaha, O., Strauss, H., 1999. 87Sr/86Sr, d13C and d18O evolution of Phanerozoic seawater. Chemical Geology. 161, 59-88.

Wiedenmayer, F., 1963. Obere Trias bis mittlerer Lias zwischen Saltrio und Tremona (Lombardische Alpen): die Wechselbeziehung zwischen Stratigraphie, Sedimentologie und syngenetischer Tektonik. Eclogae Geol.Helv. 56, 529-640.

Zanchetta, S., Garzanti, E., Doglioni, C., Zanchi, A., 2012. The Alps in the Cretaceous: a doubly vergent pre-collisional orogen. Terra Nova, 24, 351-356.

Zenger, D.H., Dunham, J.B. Ethington, R.L., 1980. Concepts and Models of Dolomitization. Society of Economic Paleontologists and Mineralogists, Special Publications, 28, 320 p.

Ziegler, P. A., 1990. Geological atlas of western and central Europe, 239 pp. Shell Internationale Petroleum Maatschappij BV.

Marine and Petroleum Geology
Volume 121, November 2020, 104615 https://doi.org/10.1016/j.marpetgeo.2020.104615

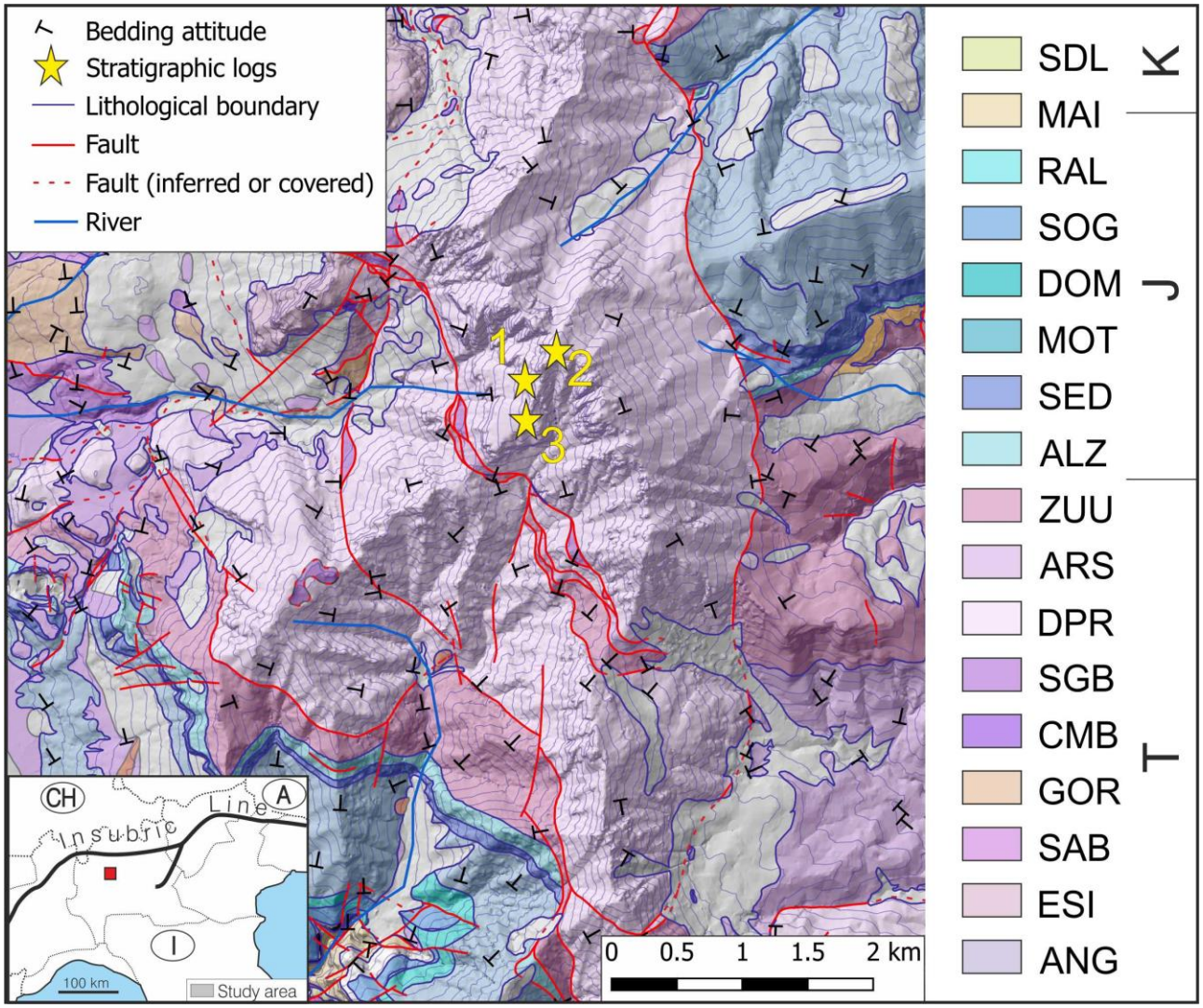

Fig. 1 Geological map of the study area (T: Triassic; J: Jurassic; K: Cretaceous; ANG: Angolo Limestone; ESI: Esino Limestone, SAB: Val Sabbia Sandstone; Gor: Gorno Fm., CMB: Calcare Metallifero Bergamasco, SGB: San Giovanni Bianco Fm., DPR: Dolomia Principale; ARS: Riva di Solto Shale; ZUU: Zu Limestone; ALZ: Albenza Fm.; SED: Sedrina Fm.; MOT; Moltrasio Limestone; DOM: Domaro Limestone; SOG; Sogno Fm.; RAL: Rosso Ammonitico Lombardo; MAI: Maiolica; SDL: Sass de la Luna). Modified after the geological map of Italy, 1:50,000 scale; ISPRA, 2012. In the inset, the red box marks the position of the study area.

Marine and Petroleum Geology
Volume 121, November 2020, 104615 https://doi.org/10.1016/j.marpetgeo.2020.104615

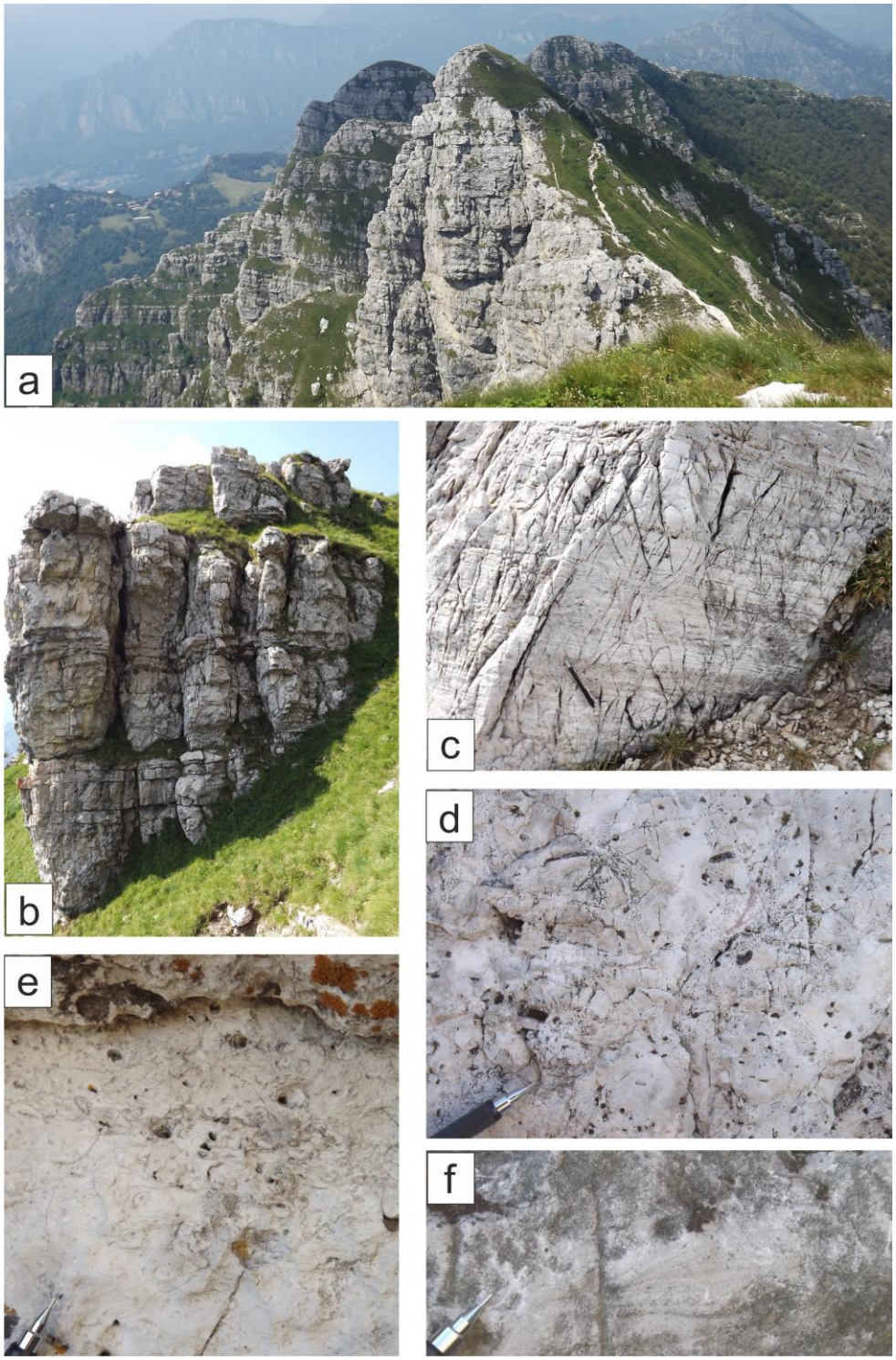

Fig. 2 - Outcrop data: a) overview the studied inner platform succession of the Dolomia Principale at Monte Resegone (the cliff is more than 150 m high); b) Detail of one of the measured stratigraphic logs (log 1 in Figure 3) where the cyclicity is well-expressed by the alternation of thin bedded (mostly intertidal stromatolite) horizons and massive (mostly subtidal) facies; the height of the cliff is about 20 m; c) dolomitized stromatolite at the top of one of the studied shallowing-upward cycles; d) fenestral fabric in a dolomitized stromatolitic bed, note the presence of pores only partly filled by dolomite cement; e) subtidal dolomitized packstone; f) laminated dolomitized packstone in a massive, subtidal bed.

Marine and Petroleum Geology
Volume 121, November 2020, 104615 https://doi.org/10.1016/j.marpetgeo.2020.104615

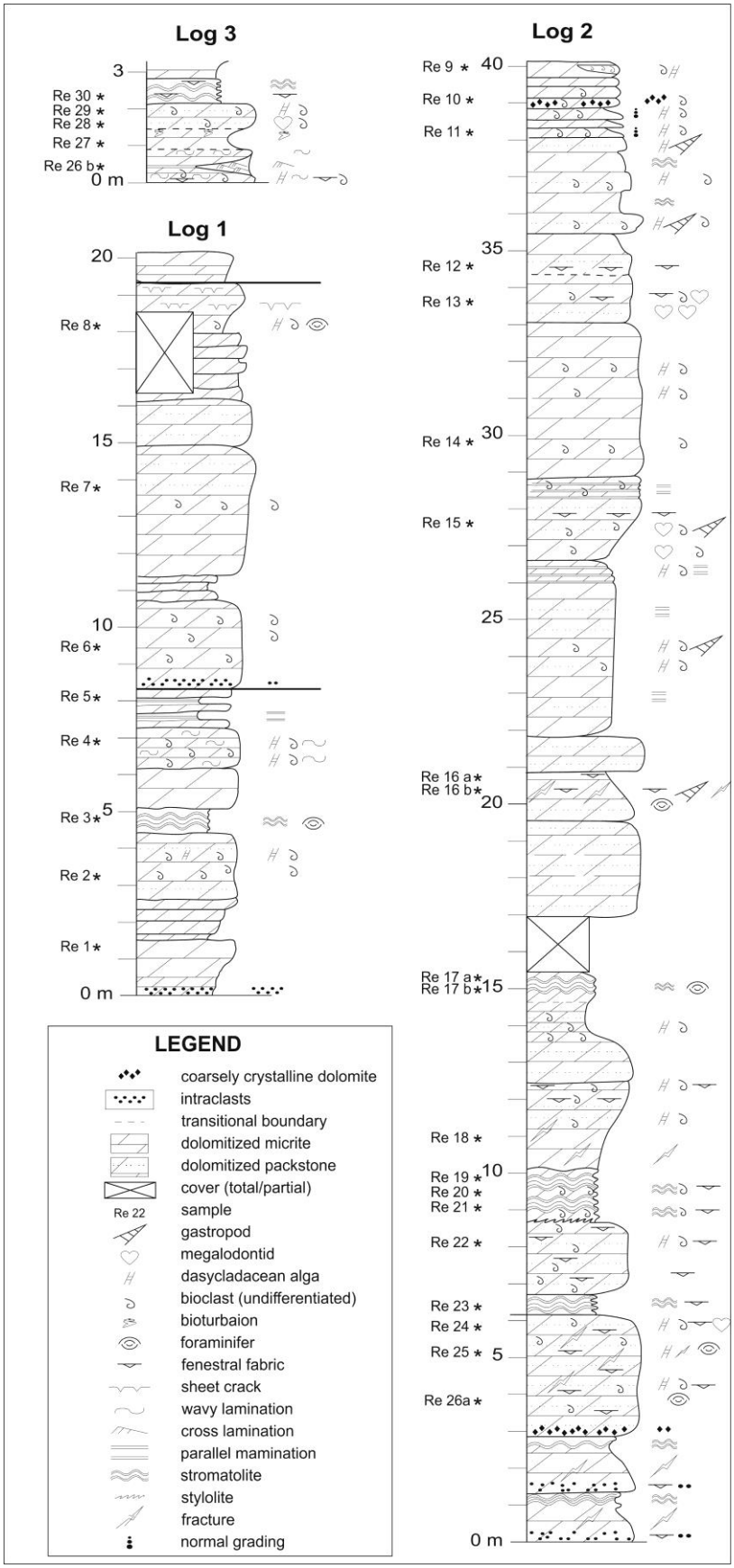

Fig. 3 – Stratigraphic logs of the Dolomia Principale at Monte Resegone (log position in Figure 1).

Marine and Petroleum Geology
Volume 121, November 2020, 104615 https://doi.org/10.1016/j.marpetgeo.2020.104615

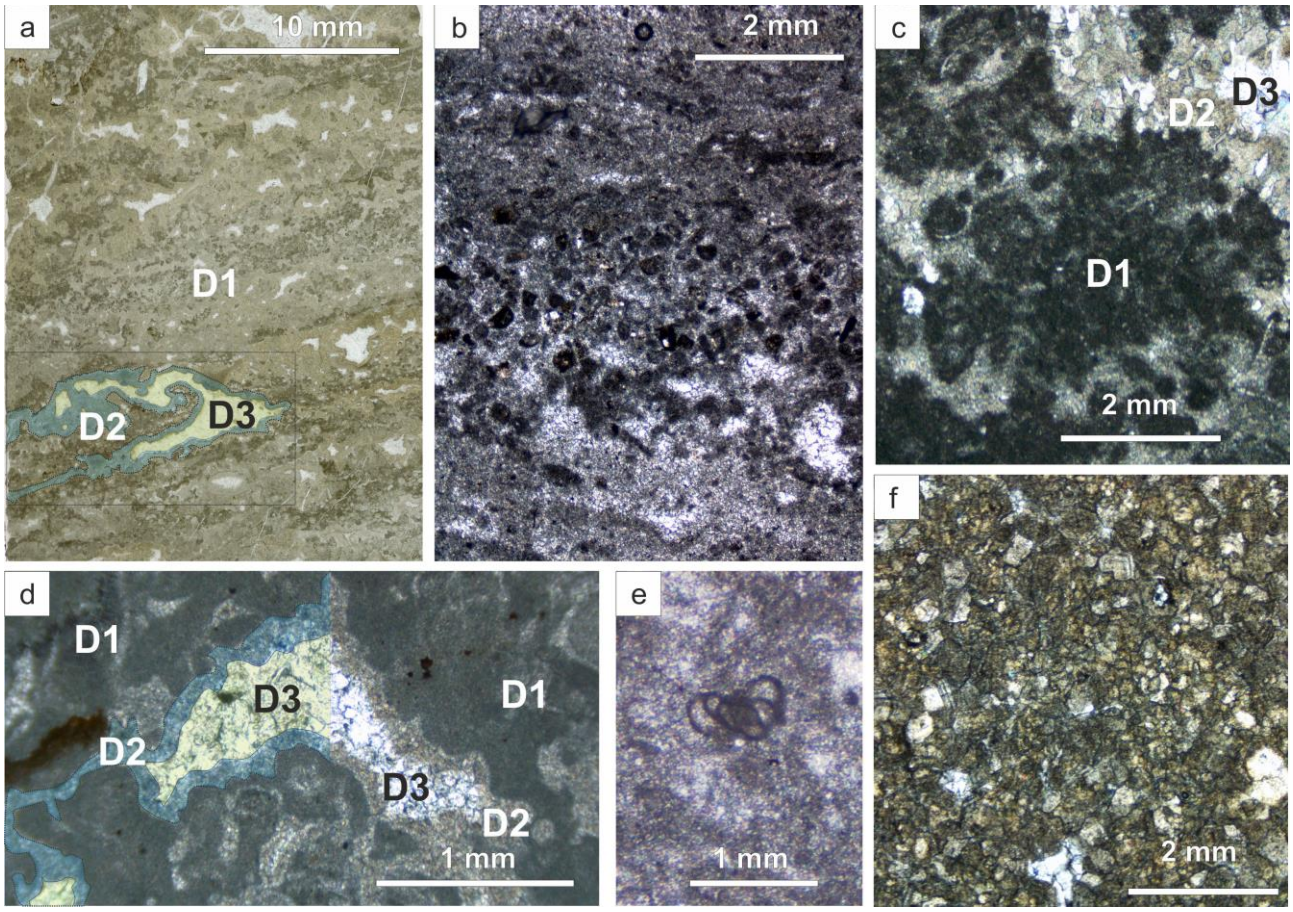

Fig. 4: Photomicrographs of thin sections from the Dolomia Principale: (a) thin section scan image of a dolomitized fenestral stromatolite (D1); the porosity is occluded by different generations of cements, typically fibrous isopachous cements (D2, an example highlighted in blue) followed by planar-s dolomite cement (D3, an example highlighted in yellow); (b) fabric-retentive dolomitized peloidal grainstone to packstone; (c) dolomitized clotted peloidal micrite (same abbreviations as in a); (d) detail of a depositional pore filled by a first rim of cloudy fibrous isopachous cement and by later planar-s dolomite cement (same abbreviations as in a); e) well-preserved benthic foraminifer in a dolomitized packstone; f) replacive fabric destructive dolomite crystals, with a cloudy core and transparent rims, completely masking the original depositional texture.

Marine and Petroleum Geology
Volume 121, November 2020, 104615 https://doi.org/10.1016/j.marpetgeo.2020.104615

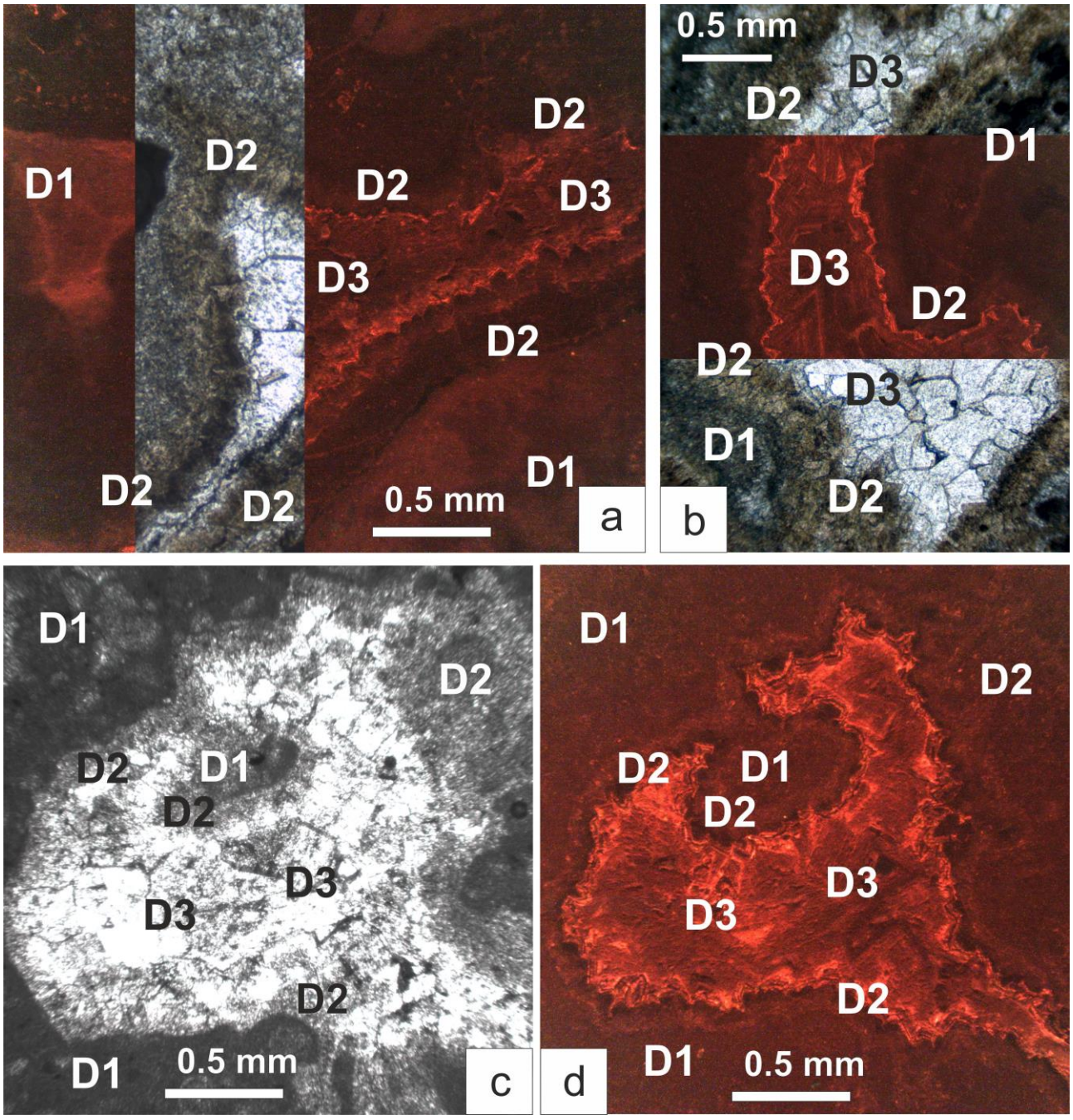

Fig. 5 Dolomite types in cathodoluminescence (a, b, c, d), showing dolomitized deposits (D1) with pores rimmed by isopachous cloudy fibrous dolomite cements (D2). D2 cements appear dull to non-luminescent under CL, supporting the interpretation as early marine cements, whose fabric is perfectly preserved (D2). The remaining porosity, not completely filled by the dolomitized early marine cements of D2, is filled by planar-s transparent dolomite cement (D3) which is brighter and zoned under CL (d) close to D2 and more homogeneous toward the center of the pores. For comparison, microphotographs in CL and transmitted light are shown.

Marine and Petroleum Geology
Volume 121, November 2020, 104615 https://doi.org/10.1016/j.marpetgeo.2020.104615

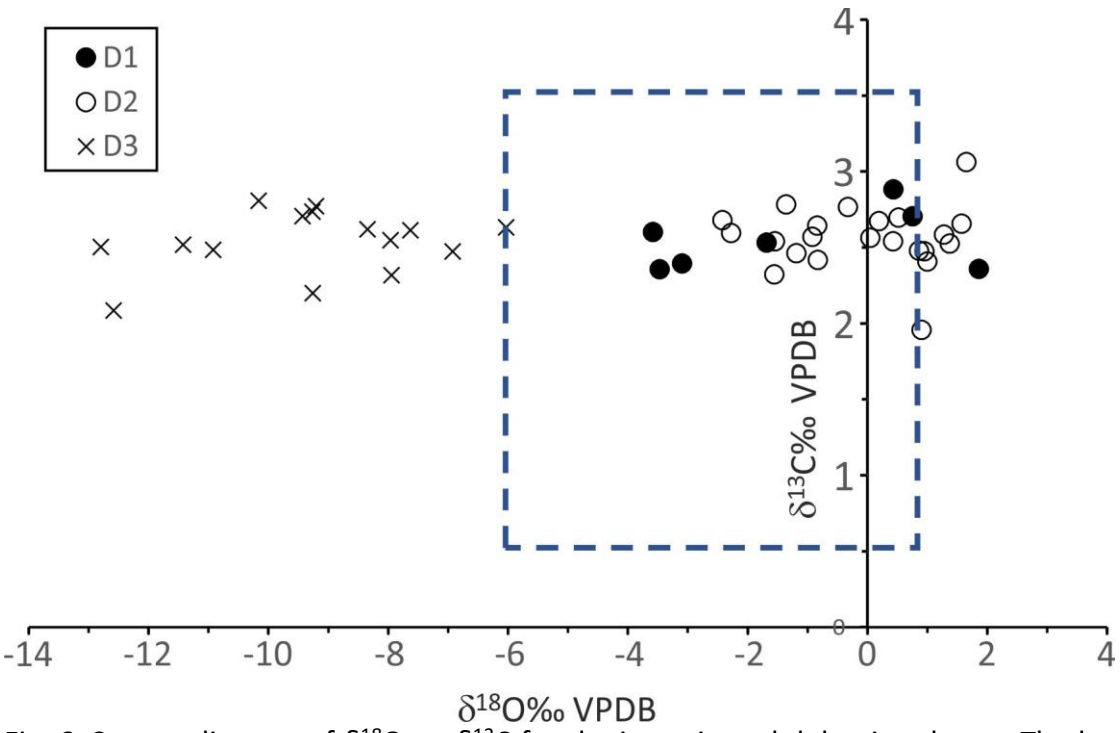

Fig. 6. Scatter diagram of $\delta^{18}O$ vs. $\delta^{13}C$ for the investigated dolomite phases. The boxes represent the range of isotopic composition of the best-preserved carbonates (mostly brachiopod shells) from the Norian seawater, estimated from different sources: red box (A) from Korte et al., 2005; dark blue (B) and light blue (C) boxes from the curves of Veizer et al., 1999, respectively with ±1 and ±2 σ.

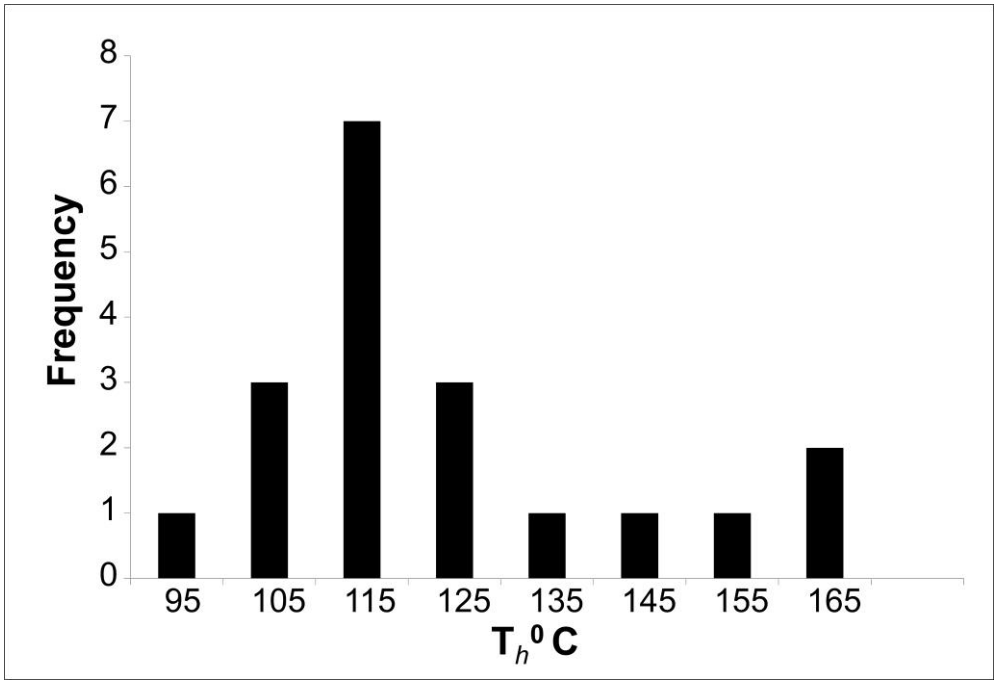

Fig. 7. Histogram of the homogenization temperatures (T_h) from fluid inclusions in D3 dolomite cement.

Marine and Petroleum Geology
Volume 121, November 2020, 104615 https://doi.org/10.1016/j.marpetgeo.2020.104615

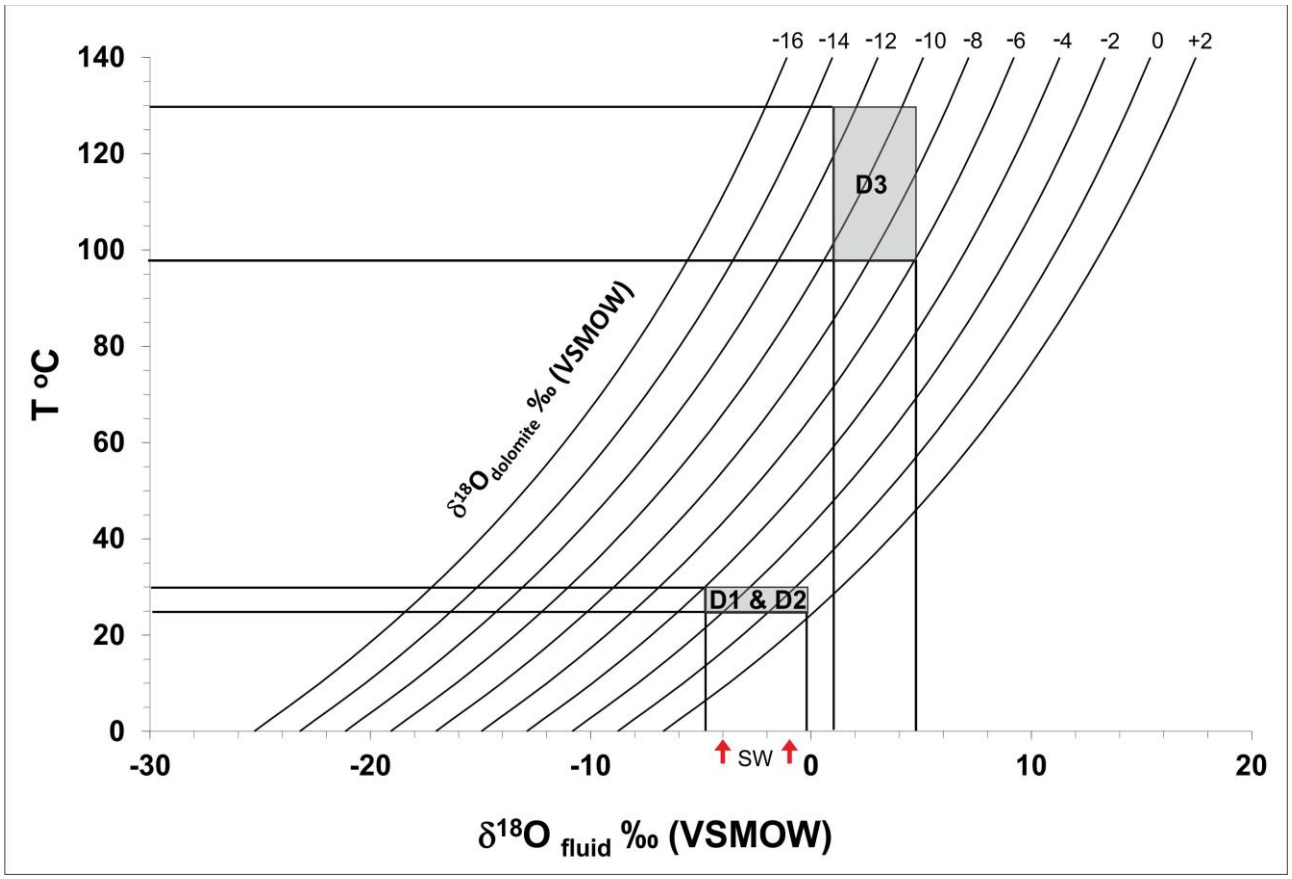

Fig. 8 Temperature (T °C) vs. $\delta^{18}O_{\text{diagenetic fluid}}$. $\delta^{18}O_{\text{dolomite}}$ values reconstructed from the equation of Land, 1983 ($10^3 \ln\alpha = 3.2\times10^6 T^{-2}-3.3$). The vertical lines mark the ranges of $\delta^{18}O_{fluid}$ based on the $\delta^{18}O_{dolomite}$ values and homogenization temperatures (T_h) of each dolomite generation. Red arrows mark the expected range of $\delta^{18}O_{SW}$ of Triassic seawater (estimated from carbonate $\delta^{18}O$ in Veizer et al., 1999 and Price et al., 2013).

Marine and Petroleum Geology
Volume 121, November 2020, 104615 https://doi.org/10.1016/j.marpetgeo.2020.104615

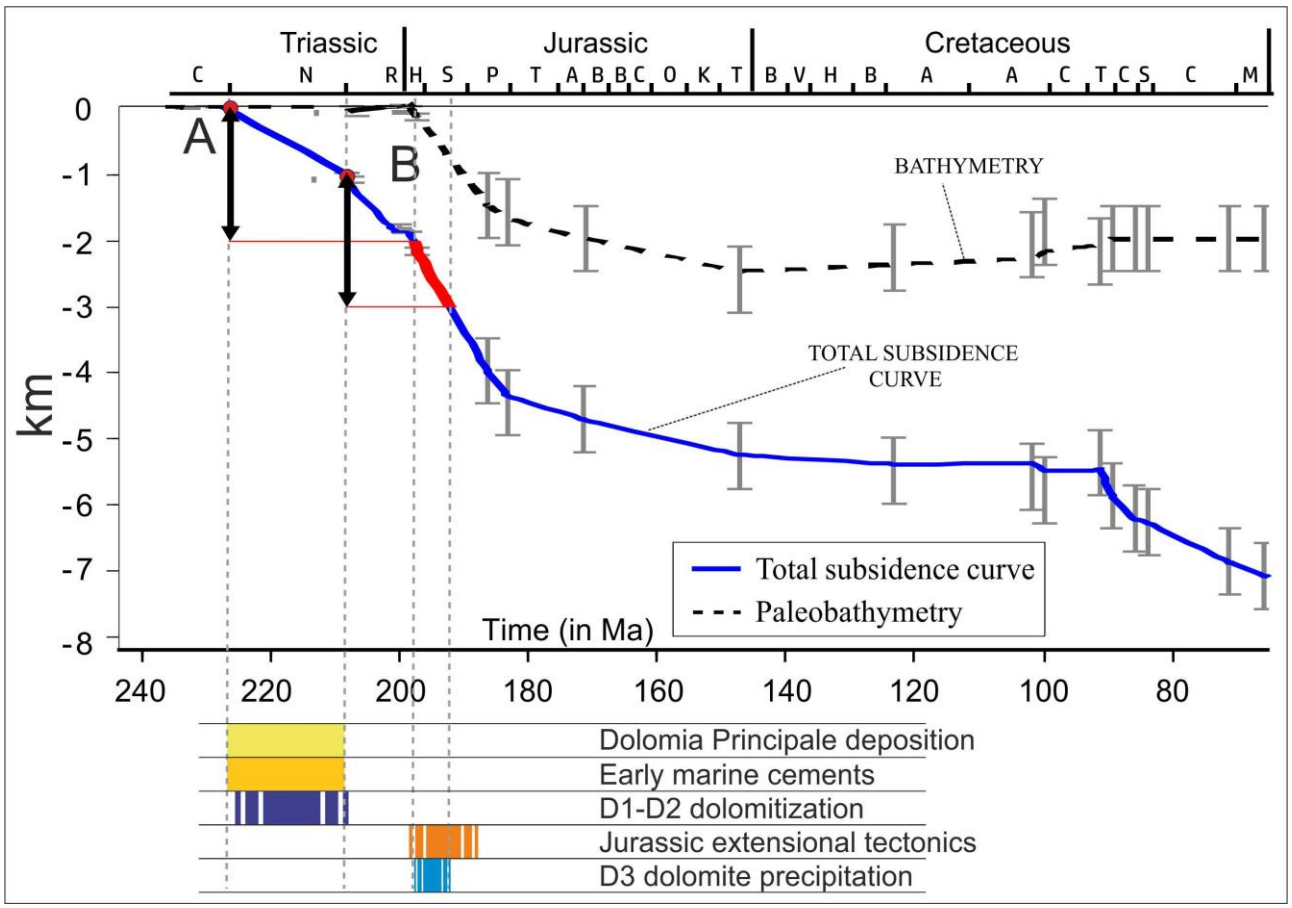

Fig. 9 - Subsidence curve from the Carnian to the Maastrichtian for the study area (Val Brembana, modified after Berra and Carminati, 2012). Red dot "A" marks the beginning of the deposition of the Dolomia Principale, the red dot "B" the end. The vertical black lines with arrows are 2 km long: it is the depth corresponding to a temperature of about 100°C considering a geothermal gradient of about 40°C/km and a surface temperature of about 25°C, required to explain the measured temperatures of homogenization. These are the minimum conditions compatible with the measured T_h from the fluid inclusions in D3. The red part of the total subsidence curve marks the deduced early Jurassic time window when D3 was precipitated filling residual primary porosity and fractures. Capital letters above the graph indicate the Triassic, Jurassic and Cretaceous stages, from Carnian (C) to Maastrichtian (M). The time interval for the precipitation of D3 is obtained considering that fluid and rocks were at the same temperature. The age of the Jurassic extensional tectonics in the Southern Alps is form different sources (e.g., Bernoulli, 1964; Bosellini, 1973; Bertotti et al., 1993; Berra et al., 2009).

Marine and Petroleum Geology
Volume 121, November 2020, 104615 https://doi.org/10.1016/j.marpetgeo.2020.104615

Table 1

Sample	Generation	$\delta^{13}C$ ‰ VPDB	$\delta^{18}O$ ‰ VPDB
RE 8 TOT	D1	2.7	0.8
RE 5 TOT	D1	2.9	0.4
RE 3 TOT	D1	2.6	-3.6
RE 26B a	D1	2.4	-3.5
RE 26B c	D1	2.4	-3.1
RE20-1	D1	2.5	-1.7
RE20-3	D1	2.4	1.9
RE13-2	D2	2.6	-0.9
RE 11 a	D2	2.0	0.9
RE 17B d	D2	2.8	-0.3
RE 17B b	D2	2.5	1.4
RE 20 a	D2	2.4	1.0
RE 24 c	D2	2.7	-2.4
RE 30 b	D2	2.5	-1.5
RE 19 d	D2	2.3	-1.6
RE 19 c	D2	2.7	0.5
RE 26A d	D2	2.4	-0.8
RE 28 c	D2	2.8	-1.4
RE30-2	D2	2.6	-0.8
RE17b-4	D2	2.5	1.0
RE19-2	D2	2.6	0.1
RE26-2	D2	2.5	0.9
RE17b-1	D2	2.7	1.6
RE30-4	D2	2.6	-2.3
RE13-1	D2	2.5	-1.2
RE26-4	D2	2.5	0.4
RE20-2	D2	2.6	1.3
RE25-1	D2	3.1	1.7
RE30-5	D2	2.7	0.2
RE 26A c	D3	2.5	-12.8
RE 24 d	D3	2.1	-12.6
RE25-2	D3	2.5	-11.4
RE 30 c	D3	2.5	-10.9
RE30-3	D3	2.8	-10.2
RE20-4	D3	2.7	-9.4
RE30-6	D3	2.7	-9.3
RE 14 c	D3	2.2	-9.3
RE19-1	D3	2.8	-9.2
RE17B-5	D3	2.6	-8.3
RE 17B a	D3	2.5	-8.0
RE 24 a	D3	2.3	-7.9
RE26-3	D3	2.6	-7.6
RE 23 b	D3	2.5	-6.9
RE17b-2	D3	2.6	-6.0

Marine and Petroleum Geology
Volume 121, November 2020, 104615 https://doi.org/10.1016/j.marpetgeo.2020.104615

Table 2

		δ^{13}C ‰ VPDB	δ^{18}O ‰ VPDB	T_h (°C)
D1	*n*	7	7	
	mean	**2.5**	**-1.3**	
	stdev	0.2	2.3	
	Max	2.9	1.9	
	Min	2.4	-3.6	
D2	*n*	22	22	
	mean	**2.6**	**-0.1**	
	stdev	0.2	1.3	
	Max	3.1	1.7	
	Min	2.0	-2.4	
D3	*n*	15	15	84
	mean	**2.5**	**-9.3**	**112.4**
	stdev	0.2	2.0	8.2
	Max	2.8	-6.0	129.5
	Min	2.1	-12.8	97.3

Marine and Petroleum Geology
Volume 121, November 2020, 104615 https://doi.org/10.1016/j.marpetgeo.2020.104615

Table 3

Sample ID	Occurrence	T_h D3
Re-28	cluster	100.0
		106.9
		116.3
		103.0
		112.8
		102.1
		117.8
		97.3
		108.3
		124.4
		115.0
		108.6
		118.3
		121.3
		119.7
		119.7
		100.7
		110.7
		126.7
		122.0
		109.8
		109.9
		102.7
Re-20	cluster	104.6
		104.6
		99.7
		104.6
		112.9
		112.9
		98.7
		110.0
		100.8
		103.0
		105.6
		108.7
		110.7
		120.9
		122.3
		122.3
		123.8
		101.7
		112.6
		121.2
		121.2
		118.5
		108.5
		108.5

Marine and Petroleum Geology
Volume 121, November 2020, 104615 https://doi.org/10.1016/j.marpetgeo.2020.104615

		108.5
		108.5
		108.5
Re-23	cluster	107.2
		115.0
		108.9
		120.1
		116.8
		102.3
		106.7
		108.4
		116.0
		122.5
		105.5
Re-14	cluster	114.3
		117.8
		129.5
		108.7
		117.3
		117.3
		128.8
		104.7
		118.9
		118.9
		122.6
		99.4
		118.1
		118.1
		118.1
		120.0
		120.0
		114.0
		114.0
		101.2
		97.6
		128.0
		109.4

n	84.0
Mean	**112.4**
stdev	8.2
max	129.5
min	97.3